Tectonophysics 493 (2010) 172–186

Contents lists available at ScienceDirect

Tectonophysics

journal homepage: www.elsevier.com/locate/tecto

Paleomagnetic evidence for clockwise rotation and tilting in the eastern Tethyan Himalaya (SE Tibet): Implications for the Miocene tectonic evolution of the NE Himalaya

Borja Antolín [a,*], Erwin Appel [a], Richard Gloaguen [b], István Dunkl [c], Lin Ding [d], Chiara Montomoli [e], Ursina Liebke [a], Qiang Xu [d]

[a] Institute for Geosciences, University of Tübingen, Sigwartstrasse 10, 72076 Tübingen, Germany
[b] Department of Geology, Technical University of Freiberg, Bernhard-von-Cottastrasse 2, 09596 Freiberg, Germany
[c] Sedimentology and Environmental Geology, University of Göttingen, Goldschmidtstrasse 3, D-37077 Göttingen, Germany
[d] Institute of Tibetan Plateau Research, Chinese Academy of Sciences, Shuangqing Rd. 18, Beijing 100085, China
[e] Department of Earth Sciences, University of Pisa, via S. Maria 53, 56126 Pisa, Italy

ARTICLE INFO

Article history:
Received 26 January 2010
Received in revised form 10 July 2010
Accepted 20 July 2010
Available online 30 July 2010

Keywords:
Tethyan Himalaya
Paleomagnetism
Pyrrhotite
SE Tibet
Miocene
Tectonics

ABSTRACT

Crustal movement around and away from the Namche Barwa syntaxis is indicated in the Asian velocity field inferred from GPS data and Quaternary fault slip rates. Nevertheless, there is a limited field-based control on the rotational history of the north-eastern Himalayan arc. Exploring the poly-phase nature of deformation, within the Cretaceous diorite dykes and their host-rock (Triassic flysch), in the eastern Tethyan Himalaya (90°–92°E), combined with new remote sensing data and existing thermo-geochronological data, allow us to unravel the kinematic relationship between paleomagnetic remanence vectors and the deformation phases. Decay at 325 °C in high temperature susceptibility curves and in the thermal demagnetization of the SIRM indicate that the characteristic remanent magnetization in the Cretaceous diorite dykes is carried by pyrrhotite. The pyrrhotite component unblocks at 280–350 °C, revealing normal and reverse polarities. It is of post-folding origin with a mean remanence direction of 019°/28° and 001°/20° in the eastern (Qonggyai valley) and western (Nagarze) part of the sampling area, respectively. The ~22 Ma K–Ar age of the last metamorphic event support that the remanence is post-Eohimalayan folding and likely of thermoremanent or thermo-chemical origin. Comparison of the declination with respect to the Early-Miocene reference direction, yields a trend from no apparent rotation in the west to 20° clockwise rotation in the east with respect to the stable Indian plate. This result can be kinematically related to the Middle to Late-Miocene strain partitioning between far-field southeast extrusion of SE Tibet and near-field strike-slip faulting and E–W extension. Furthermore the observed pattern of tilting around horizontal axis may reflect concealed North Himalayan doming.

1. Introduction

The indentation of the Indian plate into the Eurasian plate and ongoing north–south convergence of both continents resulted in large-scale shortening of Greater India (Ali and Aitchison, 2005) and the rise of the Himalayan belt around ~55 Ma (e.g. Gaetani and Garzanti, 1991; Guillot et al., 2003; Liebke et al., in press). Since these two tectonic plates collided three simplified mechanisms have controlled the Himalayan architecture: N–S shortening, N–S extension and orogen-parallel extension (Searle, 1996; Hodges, 2000; Yin and Harrison, 2000 for reviews). How these end members processes are partitioned along time plays a key role for the interpretation and modeling of the uplift of the Himalaya and the Tibetan plateau.

The present study focuses on SE Tibet, a cornerstone area in the kinematic evolution of the Himalaya–Tibet system because of its structural position in between two tectonic domains: the Himalayan domain, controlled by N–S shortening and E–W extension (since Middle Miocene; e.g Armijo et al., 1986; Jessup et al., 2008), and the Tibetan domain governed by ESE–WNW extension and southeastward and eastward movement of crustal material (since Middle Miocene, e.g. Tapponnier et al., 1982; Royden et al., 1997; Zhang et al., 2004). The far east of southern Tibet, close to the eastern Himalayan syntaxis, is a region where the indentation of India presently creates strong lateral inhomogeneity of deformation (Armijo et al., 1989; Royden et al., 1997; Holt et al., 2000). Eastward motion is evident by GPS velocities which indicate motion around and away from the

* Corresponding author. Tel.: +49 70 71/29 78931; fax: +49 7071 29 5842.
E-mail addresses: borja.antolin@uni-tuebingen.de, borjapinzas@hotmail.com (B. Antolín), gloaguen@geo.tu-freiberg.de (R. Gloaguen), istvan.dunkl@geo.uni-goettingen.de (I. Dunkl), dinglin@mail.igcas.ac.cn (L. Ding), montomoli@dst.unipi.it (C. Montomoli).

0040-1951/$ – see front matter © 2010 Elsevier B.V. All rights reserved.
doi:10.1016/j.tecto.2010.07.015

eastern syntaxis (e.g. Gan et al., 2007; Fig. 1a). However, there is currently limited field-based studies on the rotational history of the eastern Himalayan arc (Li and Yin, 2008), which can be utilized to constrain the mechanisms that have controlled part of the kinematic evolution of the eastern Himalayan Belt and SE part of the Tibetan plateau. The present study utilizes new measured paleomagnetic remanence directions, widely proved as a powerful tool in distinguishing between different kinematic models of deformation in orogens (Weil and Sussman, 2004), e.g. Apalachian mountains (Eldredge et al., 1985), Pyrenees belt (Oliva-Urcia and Pueyo, 2007); Patagonian orocline (Maffione et al., 2009). In the Himalayan orogen paleomagnetism has been applied to quantify vertical-axis block rotations in the western Himalaya reflecting the indentation of India into Eurasia and the development of the western syntaxis. The block rotation pattern in the western syntaxis describes a clockwise rotation in the eastern zone of the syntaxis and counterclockwise rotations in the western part since remanence acquisition at ~50–40 Ma (Klootwijk et al., 1985; Appel et al., 1995; Schill et al., 2001). These results have been utilized to interpret the mechanism of the formation of the Nanga Parbat Haramosh syntaxis as pure-bending, also called oroclinal bending (Schill and Holt, 2004). Further to the east (western to central Nepal) Schill et al. (2004) obtained an increasing trend to clockwise rotations in the Tethyan Himalaya remanence directions from Hidden valley in the west (83.6°E) to Shiar valley in the east (85.1°E), for remanence acquisition ages ~30–25 Ma (Fig. 1b). This was interpreted as a result of a large-scale dextral shear zone associated with the eastward extrusion of the Tibetan plateau (Schill et al., 2004). Further to the east between the Shiar valley and the study area there are no paleomagnetic data published until present.

In this paper, we report new paleomagnetic results from the Cretaceous diorite dykes widely exposed within the Triassic flysch in the eastern Tethyan Himalaya (90°–92°E). These are combined with structural data, remote sensing analysis and the existing K–Ar geochronology, Kübler Index (illite crystallinity) and vitrinite reflectance data from the Triassic flysch. Outcome from these sources provide vertical-axis block rotations and tilt around the horizontal axis to constrain the Miocene kinematic evolution and deformation mechanisms in the NE Himalayan region.

2. Geological setting

2.1. Boundaries and deformation of the Tethyan Himalayan sequence

The study area is located in the eastern Tethyan Himalayan sequence (THS) in SE Tibet, between the north dipping normal faults of the South Tibetan Detachment System (STDS) (e.g. Pêcher et al., 1991; Burchfiel et al., 1992; Carosi et al., 1998) and the Indus Yarlung suture zone (IYSZ) (Gansser, 1964; Fig.1b). The THS is the cover of the Greater Himalayan sequence (GHS) which has been probably exhumed during contemporaneous normal-sense ductile shearing along the STDS and the south-vergent thrusting on the Main Central Thrust (MCT) (Burchfiel et al., 1992; Grujic et al., 2002) at about 24–12 Ma for the whole Himalaya (Godin et al., 2006 and references therein).

The IYSZ is complexly affected by the development of the Gangdese Thrust system, the Great Counter Thrust (GCT) and locally strike-slip and normal fault systems (Yin et al., 1994; Harrison et al., 2000; Ding et al., 2005).

The THS represents a ~150 km wide zone comprising a stratigraphic record of sedimentation at the northern continental margin of India from Paleozoic to Eocene times (Gaetani and Garzanti, 1991; Willems et al., 1996). Despite differences between studies along different profiles, five main and common events have controlled the actual view of the structure in the THS. In geochronological order these are south-verging isoclinal folds with related axial plane foliation (Eocene to Early Oligocene; e.g. Burg and Chen, 1984; Ratschbacher et al., 1994; Hodges, 2000), north-vergent folds with

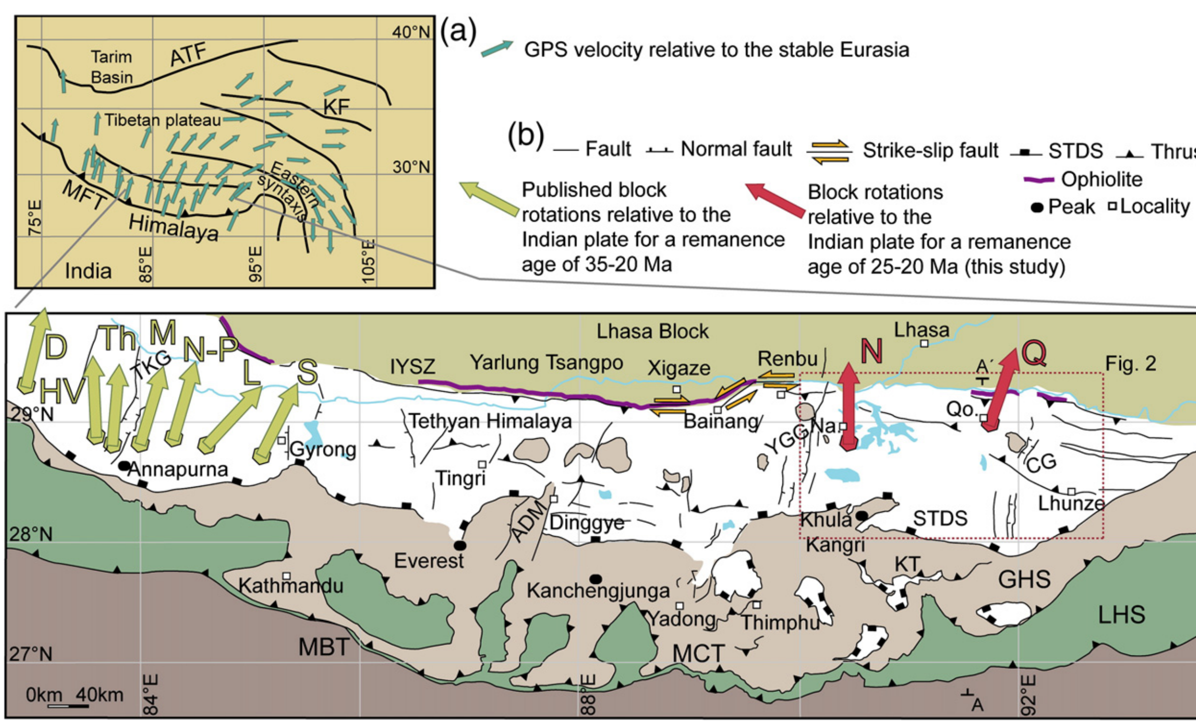

Fig. 1. a) selected and slightly generalized GPS velocity field relative to stable Eurasia (after Gan et al., 2007). MFT, Main Frontal Thrust; KF, Kunlun Fault; ATF, Altyn Tagh Fault. b) simplified geological map of the central and eastern Himalaya (after Lee et al., 2000; Pan et al., 2004; and Kellett et al., 2009) with the published paleomagnetic block rotations in the Tethyan Himalaya (Schill et al., 2004 and references therein): D, Dolpo; HV, Hidden valley; Th, Thakkhola; M, Manang; N–P, Nar/Phu; L, Larkya; S, Shiar. Paleomagnetic block rotations calculated in this study: N, Nagarze and Q, Qonggyai. TKG, Thakkhola Graben; IYSZ, Indus Yarlung suture zone; ADM, Ama Drime Massif; YGG, Yadong–Gulu Graben; Na, Nagarze; Qo, Qonggyai; CG, Cona Graben; STDS, South Tibetan Detachment System; KT, Kakhtang thrust; GHS, Greater Himalayan sequence; MCT, Main Central Thrust; LHS, Lesser Himalayan sequence; MBT, Main Boundary Thrust. Sense of strike slip-faults close to the IYSZ: South of Xigaze and in Bainang (Ratschbacher et al., 1994) and in Renbu (Yin et al., 1994).

axial plane foliation (Oligocene to Early Miocene; Godin, 2003; Montomoli et al., 2008; Kellett and Godin, 2009), top-to-the NE displacement along the STDS and north-vergent backthrusting activity on the GCT (Middle Miocene; e.g. Harrison et al., 2000; Carosi et al., 2002; Dunkl et al., in press), exhumation of the North Himalayan domes (Miocene; see Leech, 2008 for an updated review), N–S normal faults and seven major N–S-trending graben structures related to E–W extension (Late Miocene; e.g. Armijo et al., 1986; Searle, 1996; Garzione et al., 2003; Jessup et al., 2008; Fig. 1b).

2.2. Sampling and lithology of the studied area

We collected paleomagnetic samples from 30 sites in SE Tibet along two N–S profiles of about 30 km from 29°10′N to 28°54′N and separated by 130 km in E–W direction. One transect is located in Nagarze–Yamdrock Lake area (90°19′E) with 10 sites and the other in the Qonggyai valley (91°40′E) with 20 sites (Fig. 2a). The studied rocks are diorite, diabase and dolerite dykes intruded in the Triassic flysch. These dykes were sampled 15 km south of the IYSZ and 85–100 km north of STDS. The thickness of the dykes ranges from 1 m to ~100 m. The texture and the typical crystal size are very variable, changing from very coarse-grained holocrystalline to fine grained, nearly aphanitic. In the ultramafic members poikilitic or cummulate textures are typical. Some of the magmatic bodies and typically their interior parts show well conserved magmatic textures, but in many outcrops the dykes are strongly deformed and transformed to chlorite or amphibole schists. The margins and contact aureoles of the dykes are mainly alterated to banded, chaotic and mica-rich zones (Dunkl et al., in press). Close to Nagarze SHRIMP U–Pb dating of mafic dykes indicate emplacement age of 135–133 Ma (Zhu et al., 2008; Xu et al., 2009). Genesis of the studied dykes has been related to a progressive lithosphere thinning beneath eastern Gondwanaland during early Cretaceous (Zhu et al., 2008). The dykes are generally deformed within the flysch and have been affected by the main regional tectonic events above described.

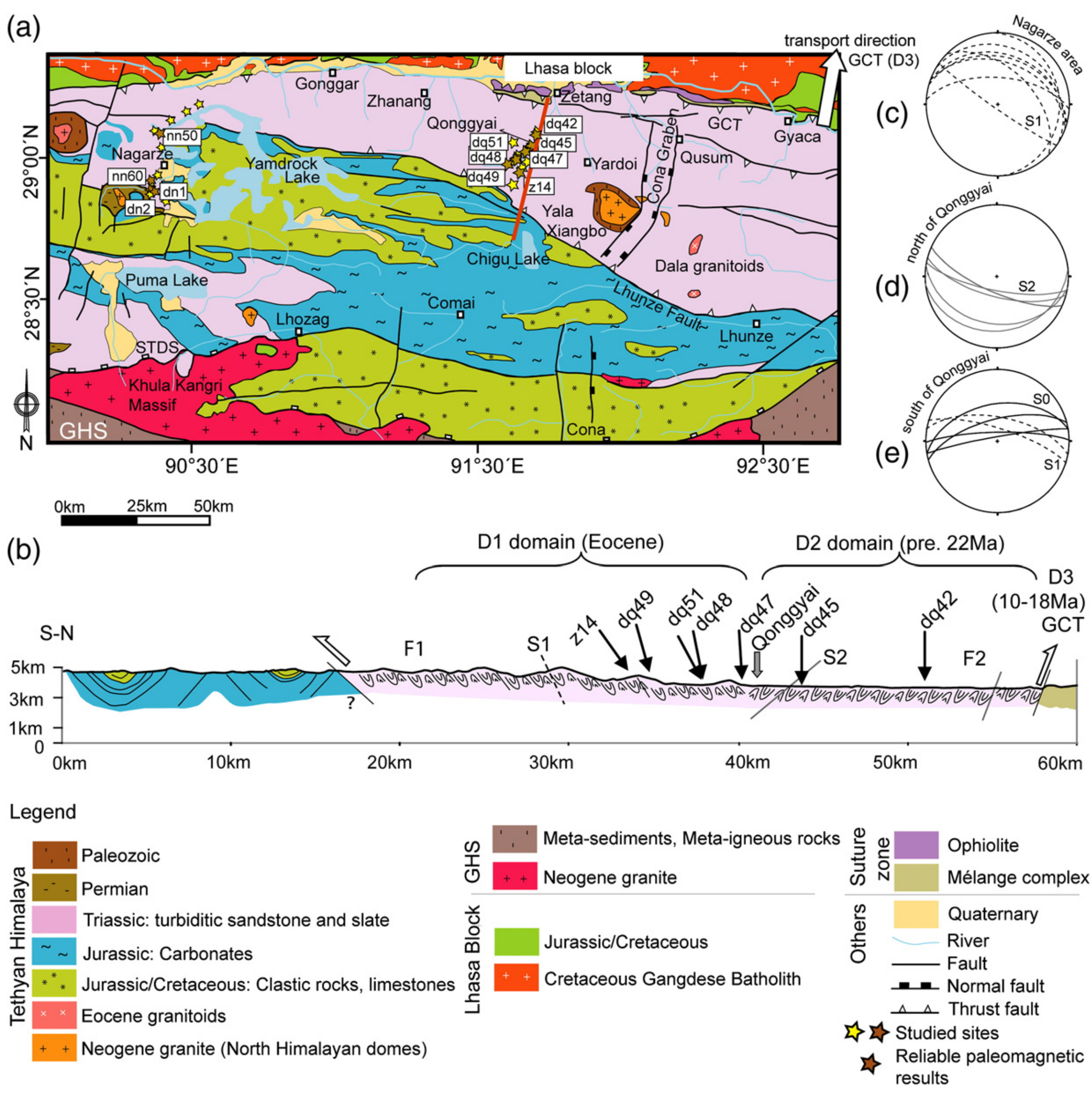

Fig. 2. a) lithotectonic map of the study area in SE Tibet after Harrison et al. (2000), Pan et al. (2004) and Aikman et al. (2008). b) cross section along the Qonggyai valley transect after map of Pan et al. (2004), Aikman et al. (2008) and data from Montomoli et al. (2008) and Antolín et al. (in press). GCT, Great Counter Thrust. STDS, South Tibetan Detachment System; GHS, Greater Himalayan sequence. c) equal-area lower-hemisphere stereogram of S1 foliation measured in Nagarze and Yamdrock lake area. d) stereogram with S2 foliation measured north of Qonggyai and east of Zetang. e) stereogram with S0 and S1 foliation measured south of Qonggyai.

2.3. Tectonic architecture and metamorphism in the Qonggyai valley

The Qonggyai valley exposes the Triassic flysch and diorite dykes along ca. 40 km between the south dipping GCT in the north and the Lhunze fault in the south (Fig. 2a,b). The GCT system brings the Triassic flysch over the mélange complex, ophiolites and Cretaceous sediments of Eurasian affinity (e.g., Yin et al., 1994; Harrison et al., 2000; Dupuis et al., 2006). The Lhunze fault trends from NW–SE to E–W and dips to the N (Aikman et al., 2008), separating the Triassic flysch (hanging-wall) from the Cretaceous and Upper Jurassic rocks (footwall). The flysch sediments, turbiditic sandstones and slates, were deposited in an abyssal and bathyal environment between Middle Triassic and Early Jurassic (Dupuis et al., 2006). South of the Lhunze fault the Cretaceous clastic rocks, limestones and Upper Jurassic continental clastic rocks, marls and marine limestones represent the platform sequence of the Indian passive margin (Fig. 2a) (Liu and Einsele, 1994; Pan et al., 2004).

The flysch pile within these two thrusts describes a double vergent wedge derived from the multi-phase tectonic history of the Tethyan Himalaya. The Triassic flysch has been affected by four main deformation phases (Fig. 3a). The southern portion, approximately

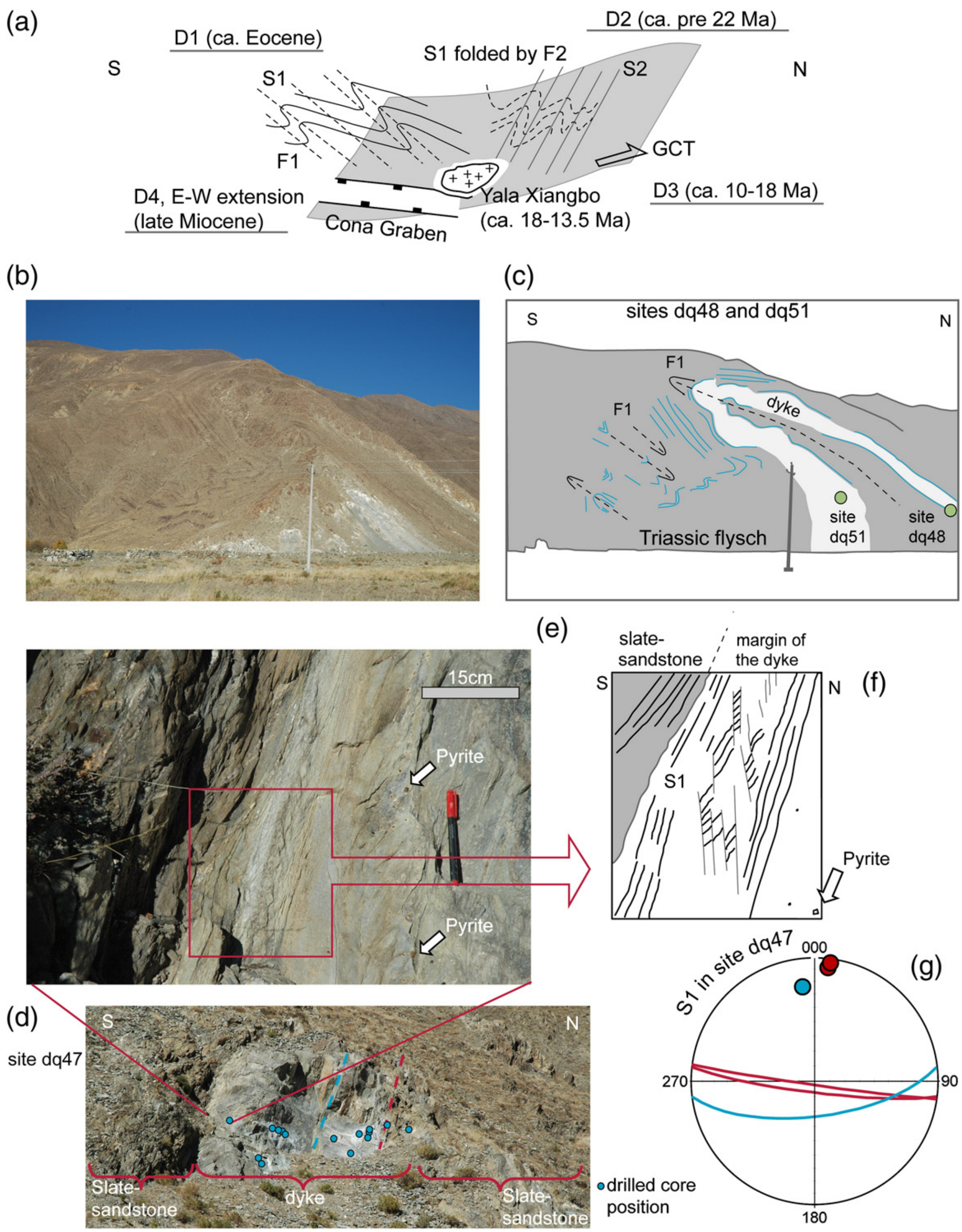

Fig. 3. a) sketch of structural relationship between deformation phases within the Triassic flysch. b and c) picture and interpretation of F1 folds close to sites dq48 and dq51. d) studied site dq47. e and f) picture of the contact between dyke and flysch and interpretation of the foliation developed in the margin of the dyke. g) equal-area lower-hemisphere stereogram of S1 foliation in site dq47.

between the Lhunze fault and Qonggyai is dominated by D1 structures typically of Eohimalayan age (Hodges, 2000). It is characterized by E–W isoclinal F1 folds and related axial planar foliation S1 trending E–W with dip to the N (Montomoli et al., 2008) (Figs. 2b,c,e and 3a). Fig. 3b shows a decametric folded diorite dyke (F1 fold) parallel to the Triassic flysch F1 folds (Fig. 3c). Stretching lineation, obtained from anisotropy of magnetic susceptibility data, south of Qonggyai trend SSW–NNE with intermediate plunges to the N and has been related to southward motion of flysch slices along thrust planes towards the Himalayan foreland in consonance with the main southward vergence of the orogen (Antolín et al., in press). Locally S1 can occur steeply dipping toward the S as in the area around Qonggyai village, due to the development of later collapse folds with sub-horizontal axial plane. Fig. 3d,g shows S1 foliation in the margin of a dyke parallel to the foliation of the neighboring slates (site dq47 in Fig. 2a,b). Moving to the north the flysch is characterized by north-vergent F2 decametric folds and microfolds which deform the S1 foliation (Montomoli et al., 2008). Approaching the GCT the flysch structure is controlled by S2 foliation trending E–W and dipping to the south, caused by hinterland propagation of the deformation (D2 deformation phase; Figs. 2d and 3a). K–Ar isotope radiogenic ages in newly grown illites near site dq45, within the D2 domain, show ~22 Ma cooling ages which have been related to peak metamorphism during the D2 phase (Dunkl et al., 2008; Antolín et al., in press). During D2 the Triassic flysch and diorite dykes underwent anchi- to epizonal metamorphic conditions, as indicated Kübler Index values (Dunkl et al., in press). Continuation of backward deformation towards higher structural levels was probably responsible for the formation of the north-directed GCT around 18 Ma to 10 Ma (D3 phase; Fig. 3a) (Yin et al., 1994; Harrison et al., 2000; Antolín et al., in press).

The Yala Xiangbo North Himalayan dome (Fig. 2a) was emplaced at ca. 18 Ma and cooled at ca. 13.5 Ma (Aikman et al., 2004). Finally orogen parallel extension (E–W) dominates the orogen architecture, which trigger kilometer-scale N-trending normal faults during the Pliocene; D4 phase (e.g. Armijo et al., 1986; Fig. 3a). The study area is bounded to the west by the Yadong Gulu Graben (90°E) and is cross-cut by the easternmost Himalayan Graben, the Cona Graben at ~92°E (Figs. 1b and 2a; Armijo et al., 1986; Garzione et al., 2003). GPS velocities indicate no significant (0.3 ± 0.9 mm/yr) fault opening at present-day in the Cona Graben and 2.0 ± 0.6 mm/yr opening rate in the Yadong–Gulu Graben (Gan et al., 2007).

3. Methods

3.1. Sampling and paleomagnetic laboratory procedure

In general 10 cores with 2.5 cm in diameter were taken from each site using a portable gasoline powered drill. A magnetic compass was used for in situ core orientation. Deviation due to rock magnetization can be considered as negligible as the content of ferromagnetic minerals in the dykes is relatively low (magnetic susceptibility averaged for 16 sites, 170 samples, is 650.1×10^{-6} SI). The declination of the ambient magnetic field was 0° during the sampling campaign period (NOAA's National Geophysical Data Centre, http://www.ngdc.noaa.gov). The cores were cut into specimens of standard size (2.2 cm length). Sampling was focused in the margin of the dykes where sulphur migration from the neighboring slates could increase the original sulphur content of the dyke and result in the formation of pyrrhotite. Two sites (dq48 and dq51) could be drilled within the limbs of a decametric isoclinal fold deformed within the Triassic flysch (Fig. 3c). Differences of foliation attitudes in the neighboring flysch and at the margin of the dykes allow tectonic correction of the sites and the application of fold tests.

Rock magnetic experiments were elaborated to determine the nature of the carrier of characteristic remanence magnetization (ChRM): Low and high temperature thermo-magnetic curves using a CS3 unit coupled with a Kappabridge KLY-3 (AGICO), acquisition curves of isothermal remanent magnetization (IRM) in a stepwise increasing DC field up to 1.9 T at room temperature using an MMPM9 pulse magnetizer (Magnetic Measurements) and stepwise thermal demagnetization of the saturation IRM (SIRM). Furthermore in 3 selected samples we performed low-temperature measurements down to 5 K in a zero field environment using a Magnetic Properties Measurement System (MPMS)-XL7 magnetometer (Quantum Design Ltd.).

Demagnetization procedures were first performed on pilot specimens (two samples per site). Alternating field stepwise demagnetization (AfD) of natural remanent magnetization (NRM) was performed using an automatic degausser (2G600) coupled to a three-axis SQUID magnetometer (RF SQUID 760 R, 2G Enterprises). This magnetometer was also used to measure the magnetization remaining after each step of heating. Stepwise thermal demagnetization (ThD) of NRM and SIRM were performed utilizing a thermal specimen demagnetizer, model TD-48SC (ASC Scientific). Susceptibility was monitored after each step of ThD to control changes in the magnetic mineralogy using a Kappabridge KLY-2 (AGICO). After comparison of the two methods, ThD was chosen for demagnetization of the bulk samples. AfD did not reach complete demagnetization and furthermore ThD showed more stable demagnetization behavior. ChRM directions for each sample were computed by principal component analysis (Kirschvink, 1980). Sites means were determined by Fisher (1953); single specimen directions with reverse polarity were inverted before averaging. Fold tests were performed after McFadden (1990). The present-day GAD direction for the sampling area was calculated by means of the program IGRF version 4. All magnetic measurements were done in the paleomagnetic laboratory at the University of Tübingen except MPMS measurements which were carried out at University of Bremen.

3.2. Neotectonic analysis

Rivers flowing along bedrock channels are the primary non-glacial mechanism of incision. The rate at which channels incise sets the rate at which the rest of the landscape evolves, and hence may control the response time of such landscapes to tectonic forcing (e.g. Jackson et al., 1996; Gloaguen et al., 2008). The drainage network is extracted from SRTM v.4 data by calculating flow directions at all points using the D8 algorithm. Stream longitudinal profiles are identified and selected based upon least cost path analyses (Shahzad and Gloaguen, in press-a). We compute paths of least down slope resistance (i.e. the downstream flow path) and Strahler's stream order. Incision maps, i.e. the local relief within a moving window, provide useful information for the determination of neotectonic features (e.g. Käßner et al., 2008). The spatial organisation of a river system and its space filling properties (e.g. dendritic and orthogonal) can be strongly controlled by tectonics (e.g. Jackson et al., 2002; Gloaguen et al., 2007). Their analysis provides first hand clues to characterize tectonic forcing on landscape formation (e.g. Burbank et al., 1996; Shahzad et al., 2009). Analysis of basin asymmetry can provide important map-scale data for neotectonic assessment, allowing the delineation of geomorphic domains of stream migration that may be related to tilting fault blocks or developing folds (e.g., Cox et al., 2001). As streams respond to uplift or subsidence by migrating laterally in a down-tilt direction, a record of this migration is preserved as an asymmetric position of the main basin river with respect to the watershed axis. This technique produces a vector field (T-factors) of spatially averaged directions of basin asymmetry (inferring lateral stream migration), and areas showing preferred directions of stream migration can be evaluated in terms of tectonic forcing. A semi-automated method of analysis which delivers the T-factor morphometric index from a Digital Elevation Model (DEM) has been implemented on MATLAB (Shahzad and Gloaguen, in press-b). From these vector data, different spatial domains can be drawn, whereas the offset directions contribute to constraint the main active strain orientation.

4. Paleomagnetic results

4.1. Rock magnetism

Rock powder samples from 11 sites, two from Nagarze and 9 from Qonggyai were analysed for susceptibility versus temperature. Low-temperature curves down to −196 °C show temperature dependence following the Curie Law (Nagata, 1961) below −100 °C, indicating small contribution of paramagnetic minerals to the total magnetic susceptibility signal. Low-temperature curves down to 5 K carried out in the MPMS did not show Morin transition of hematite at ~260 K, Verwey transition of magnetite at ~120 K, or pyrrhotite transition at 30–34 K (Rochette et al., 1990; Fig. 4a). High-temperature curves indicate that magnetic susceptibility is predominantly controlled by the existence of pyrrhotite pointed out by a Hopkinson peak followed by a marked drop of susceptibility around the Curie temperature of pyrrhotite at ca. 325 °C (Fig. 4b, dq47 and dn5). At higher temperature of >400 °C a rise in magnetic susceptibility indicates the new formation of magnetite due to heating. Some samples indicate also a contribution of initial magnetite indicated by a decay of susceptibility around the Curie temperature of magnetite ca. 580 °C (Fig. 4b, dq42).

IRM starts to saturate from 300 to 500 mT until 1 T when saturation is almost reached (Fig. 4c). Such saturation fields are clearly higher than expected for magnetite (max. 300 mT) and typical for pyrrhotite. Thermal demagnetization of SIRM is mainly achieved around the Curie temperature of pyrrhotite (325 °C) in all the studied samples and afterwards a minor decay at around 580 °C indicates a small contribution of magnetite (Fig. 4d).

These results confirm the existence of pyrrhotite as the major ferro(i)magnetic phase in the studied dykes. Surprisingly despite the clear existence of pyrrhotite in e.g. high-temperature curves and thermal demagnetization of SIRM there is no low temperature transition observed at 30–34 K in the MPMS analyses. Occurrence of pyrrhotite as a remanence carrier within the Tethyan Himalaya has been widely demonstrated in low-grade metacarbonates of the western and central Himalaya providing stable and meaningful remanence directions (Rochette et al., 1990; Appel et al., 1995; Schill et al., 2004).

Measured magnetic susceptibility after each step of heating during thermal demagnetization indicates no significant changes of the magnetic susceptibility below the Curie temperature of pyrrhotite. Some of the samples exhibit an increase of the magnetic susceptibility above 400 °C, likely indicating the transformation of the initial pyrrhotite and pyrite into magnetite as previously pointed out by Crouzet et al. (2001).

4.2. Remanence directions

Thermal demagnetization with detailed stepwise heating around the Curie temperature of pyrrhotite (10 °C steps from 270 °C to 350 °C) was performed in order to determine the pyrrhotite component. About 50% of the studied sites show no stable components. For the other sites common rock magnetic properties and sufficiently clear demagnetization behavior permit to separate a stable component in most of the samples within the pyrrhotite unblocking temperature range of 280 °C to 350 °C (Fig. 5).

In total 11 sites, 7 in Qonggyai valley and 4 in Nagarze area, show a consistent demagnetization behavior and reliable components could be extracted from the Zijderveld diagrams. Remanence directions show normal and reverse polarity (Fig. 6a,e). In some of the sites

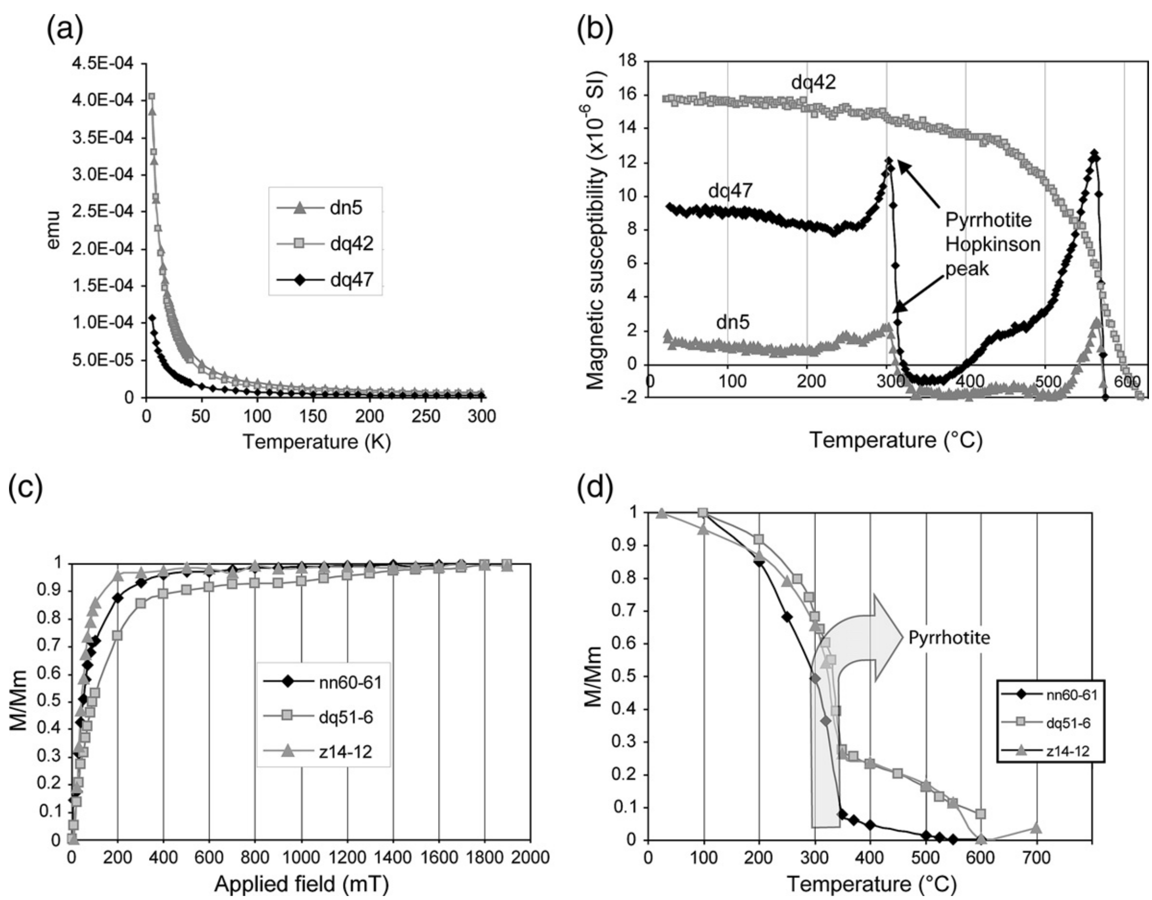

Fig. 4. Rock magnetism experiments. a) MPMS low-temperature curves. b) high-temperature curves of magnetic susceptibility versus temperature. c) stepwise IRM acquisition. d) thermal demagnetization of SIRM (pyrrhotite unblocking indicated).

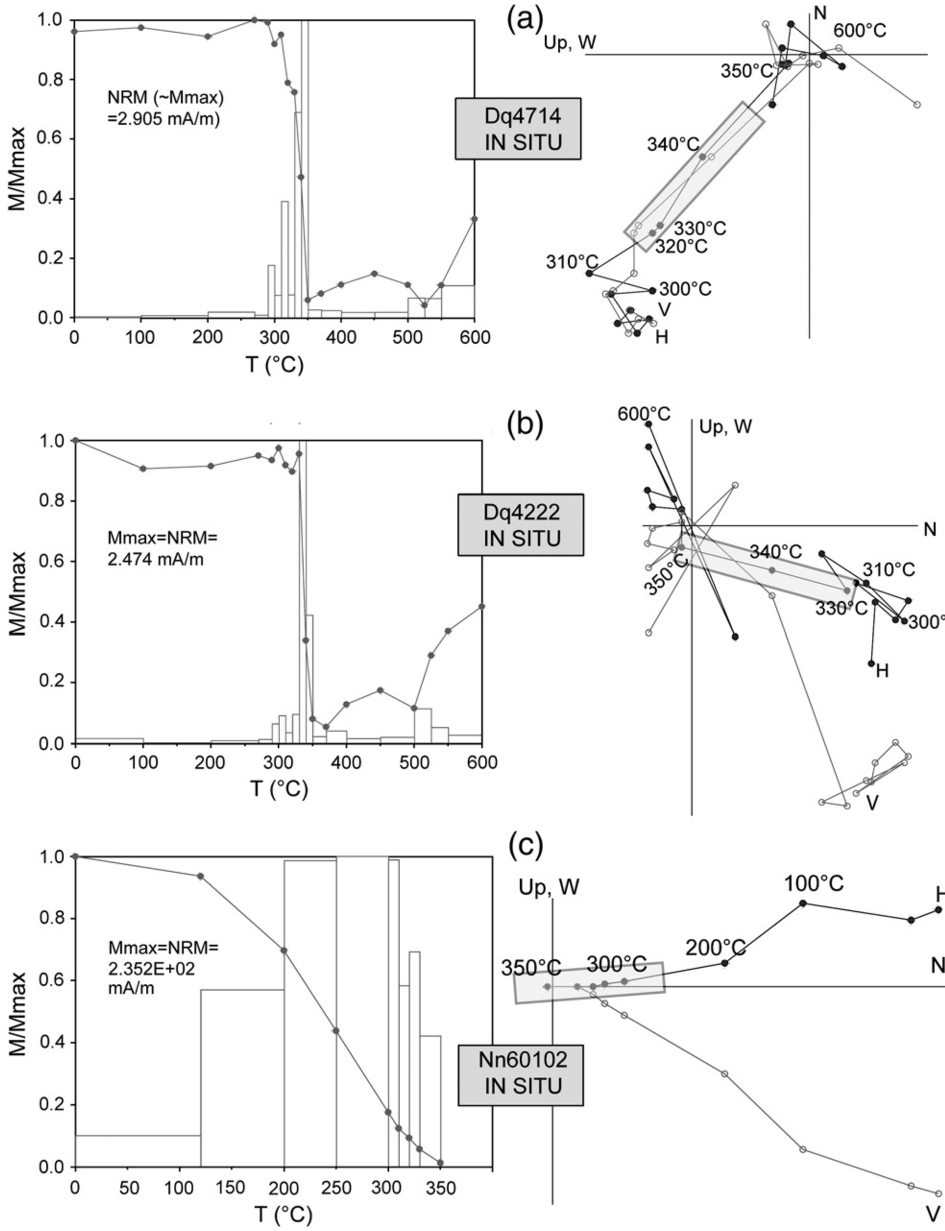

Fig. 5. Thermal demagnetization of NRM for representative specimens from sites dq47 (a), dq42 (b) and nn60 (c). Intensity curves (left) and orthogonal Zijderveld plots (right) are shown; the main unblocking range is indicated.

several components can be isolated in the range of the unblocking temperature of pyrrhotite and in most of the cases they show similar (anti-parallel) directions.

In Qonggyai valley 7 sites, equally distributed along the profile, indicate the presence of one stable pyrrhotite component; reliable directions were obtained for a significant number of samples ($n = 73$) (Figs. 2a and 5a,b). The site means directions have $6.6 < \alpha_{95} > 22.1$ and $k > 10$ (except in site dq51, $k = 5.2$) indicating good grouping of the intra-site remanence directions (Table 1, Fig. 6b). This component shows an approximate constant declination of ca. 019° (geographic coordinate system; normal polarity) along 30 km of the double vergent flysch wedge as can be seen in the stereogram of the site mean vectors and in the density plot of ChRM directions of all specimens (Fig. 6b,c,d). Inclination values are ranging from 50° to 10° (Table 1, Fig. 6b). Fold test (McFadden, 1990) using foliation attitudes of the D1 deformation phase domain (sites z14 and dq47) and the D1 and D2 domain (sites z14 and dq42) support a post-folding origin of the remanence (Fig. 7). The fold test for the D1 domain shows that the magnetization was probably acquired at 0% of "unfolding" (Fig. 7a,b,c). The fold test applied in the D1 + D2 domain yields the best k grouping at −22% of unfolding (Fig. 7d,e,f).

In Nagarze area the demagnetization behavior is similar as in Qonggyai valley and 4 sites (28 samples) exhibit pyrrhotite unicomponents (Figs. 2a and 5c). The specimen directions within sites are more scattered than in the Qonggyai valley (Fig. 6e), but the 4 sites show similar site mean declinations (Table 1, Fig. 6f,g). The directional maxima in the density plot appear at declination 001° (Fig. 6f,g). Inclinations show lower values than in Qonggyai valley ranging from 30° to 6° (Table 1, Fig. 6f). No fold test could be applied for the Nagarze area as no folded dykes were sampled and the D1 foliation shows similar attitudes in all the sites.

5. Timing of remanence acquisition and paleomagnetic reference directions

Peak metamorphic conditions are crucial to the formation of pyrrhotite and secondary remanence acquisition. Metamorphic ages (K–Ar) from newly grown illites in the Triassic flysch along the

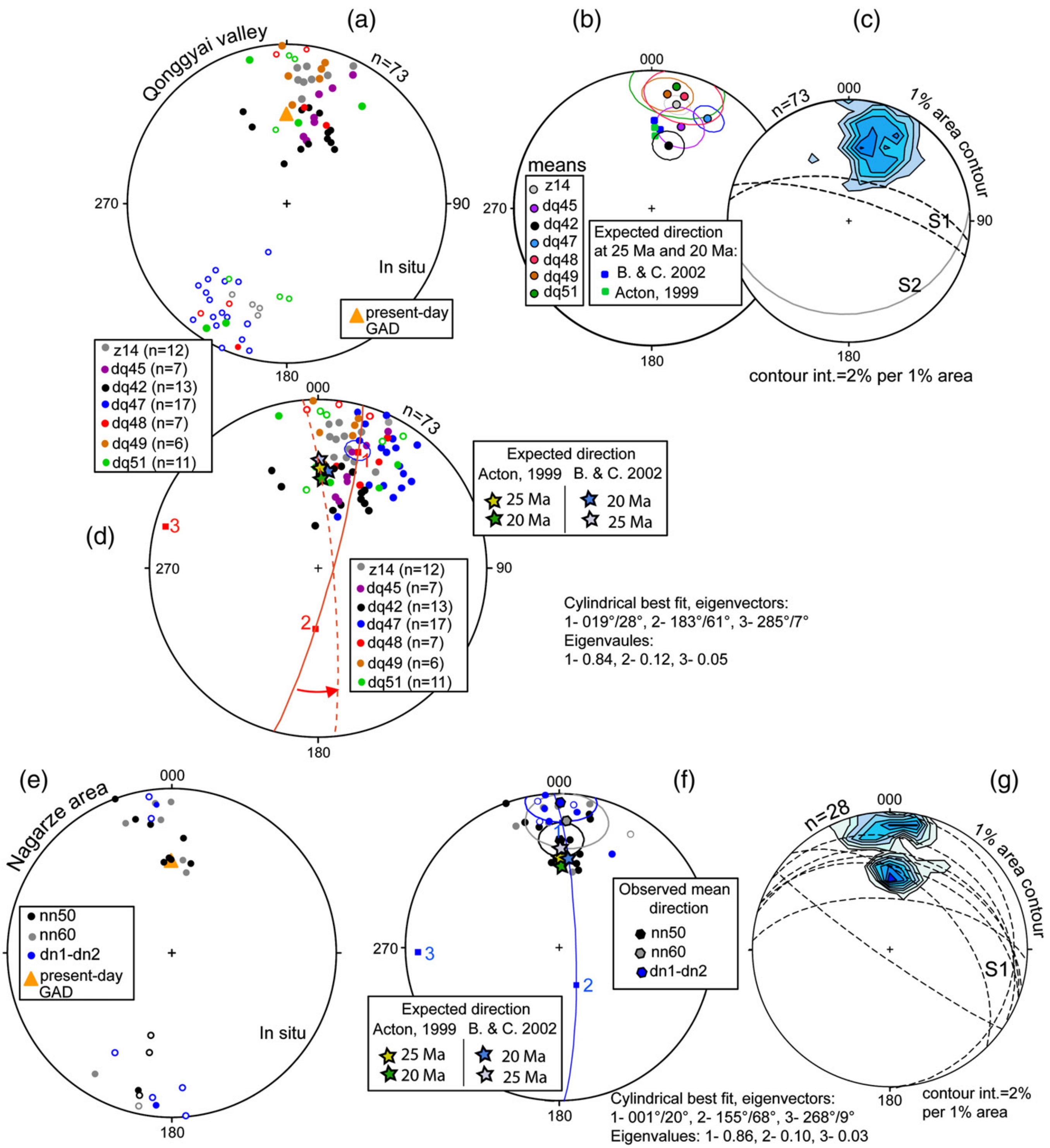

Fig. 6. Paleomagnetic results in the Qonggyai valley and Nagarze area (all stereograms are in equal-area projection). a) single specimen pyrrhotite directions and present-day GAD for Qonggyai valley. b) mean site directions in Qonggyai valley and expected directions from the APWPs of Acton (1999) and Besse and Courtillot (2002). c) density plot stereogram of single specimen ChRM components and general trend of S1 and S2 foliation. d) single specimen directions (reverse polarities were inverted) with cylindrical best fit; open (solid) circles are projected in the upper (lower) hemisphere. e) single specimen directions and present-day GAD for Nagarze area. f) in situ mean directions in Nagarze (hexagons); single specimen directions (reverse polarities were inverted), open (solid) circles are projected in the upper (lower) hemisphere; expected directions from the two APWPs (stars) and cylindrical best fit. g) density plot stereogram of single specimen ChRM components and S1 foliation planes.

Qonggyai valley indicate that the last metamorphic peak was at ~22 Ma, associated with the end of the D2 tectonic phase (Dunkl et al., 2008). Illite Kübler Index in the Triassic flysch of Qonggyai valley ranges from 0.17 to 0.39 and vitrinite reflectance values vary from 1.84% to graphite grade (for details see Dunkl et al., in press). Near Qonggyai town vitrinite reflectance values indicate the highest level of maturation reaching graphite stage (Rmax~9%), and the dykes have been transformed to greenschist. Paleotemperature estimates from these values yield maximum temperatures between 200 °C and lower greenschist facies (biotite-in ca. 450 °C; Dunkl et al., in press). Thus we suppose a thermoremanent or thermo-chemical origin of the pyrrhotite remanence related to the Early-Miocene temperature

Table 1
Statistical parameters for the pyrrhotite component. S.D, structural domain; D1, domain controlled by D1 deformation phase; D2, domain controlled by D2 deformation phase. Foliation, dip direction/dip (DD/D), of the flysch host-rock. n, number of specimens measured/number of specimens included in statistics. norm./rev., normal/reverse polarities. In situ mean remanence directions: D/I, declination/inclination in geographic coordinates; k, precision parameter; α_{95}, 95% confidence angle. After tectonic correction: D/I, declination/inclination. Rot., rotation angle calculated from the expected direction at 20 and 25 Ma obtained in the APWPs of A.99 (Acton, 1999) and BC. 02 (Besse and Courtillot, 2002). T.H.A, tilting angle around a horizontal axis at 20–15 Ma; positive/negative values denote downward/upward tilt.

Sites	Geographic coordinates		S. D.	Foliation	n	Polarity	In situ				After tectonic correction	Rot. at 20 Ma		Rot. at 25 Ma		T.H.A.
	Latitude °N	Longitude °E		DD/D		no./re.	D/I	k	α95 (°)	α95/cosI (°)	D/I	A.99 (°)	BC. 02 (°)	A.99 (°)	BC. 02 (°)	(°)
dq42	29.0860	91.7048	D2	186/56	13/20	13/0	14.9/50.7	22.5	8.9	14.1	167.9/71.7	13.0	9.4	13.5	13.8	13.8
dq45	29.0450	91.6875	D2	186/56	7/18	7/0	19.6/37.4	22.0	13.1	16.5	117/78.5	17.7	14.1	18.2	18.5	1.4
dq47	29.0261	91.6704	D1	183/79	17/31	0/17	32.1/24.1	20.0	8.2	9.0	122.2/59.4	30.2	26.6	30.7	31.0	−11.9
dq48	28.9971	91.6335	D1	14/68	7/24	3/4	16.3/15.9	10.9	19.2	19.9	17.6/−52	14.4	10.8	14.9	15.2	−20.1
dq49	28.9783	91.6068	D1	14/68	6/18	6/0	7.9/17.3	30.7	12.3	12.9	4.9/−50.2	6.0	2.4	6.5	6.8	−18.7
dq51	28.9954	91.6340	D1	14/68	11/25	5/6	11.7/10.8	5.2	22.1	22.5	9.8/−57.1	9.8	6.2	10.3	10.6	−25.2
z14	28.9494	91.6485	D1	353/70	12/12	8/4	13.8/23.8	44.8	6.6	7.2	18.9/−41.8	11.9	5.7	12.4	10.1	−12.2
nn50	29.0925	90.3929	D1		12/20	9/3	1.1/30.1	18.4	10.4	12.0		−0.8	−4.4	−0.3	0.0	−5.9
nn60	28.9202	90.4808	D1	20/40	8/16	6/2	3.5/17.8	10.6	17.9	18.7	3.2/−20.6	1.6	−2.0	2.1	2.4	−18.2
dn1+dn2	28.8832	90.3729	D1	4/59	8/19	2/6	0.8/5.4	16.6	14.0	14.1	358.6/−53.5	−1.1	−4.7	−0.6	−0.3	−30.6

climax or/and subsequent cooling. Alternatively the origin of the pyrrhotite remanence can be related to Miocene granitic bodies cropping out in the core of the North Himalayan domes (e.g. Hodges, 2000; Lee et al., 2000), producing local thermo-metamorphism in the Triassic sediments. In the study area two Neogene granitoids outcrop in Nagarze area and one SE of Qonggyai within the Yala Xiangbo North Himalayan dome (Fig. 2a). The Yala Xiangbo dome was emplaced at ~18 Ma, and cooled through the muscovite closure window at ~13.5 Ma (Aikman et al., 2004).

Sulphur provenance for pyrrhotite formation is supposed to come from the organic material of the pelites during diagenesis and metamorphism. Pyrrhotite could also be formed by the transformation of pyrite or magnetite (Crouzet et al., 2003 with references). Pyrite is widely present in the margin of the dykes and small amounts of magnetite have also been found after magnetic mineralogy analysis which could mark this transformation.

The Early-Miocene age of remanence acquisition is in agreement with the negative fold test found for the D1 deformation phase domain and the D1 + D2 domains at Qonggyai valley (Fig. 7). This indicates that the remanence acquisition was post-folding F1 folds of Eohimalayan age and post F2 folds and S2 foliation or synchronous with the last pulses of the D2 tectonic phase (~22 Ma). The pyrrhotite ChRM directions differ from the present-day GAD direction (Fig. 6a,e). To quantify the amount of vertical-axis rotation and tilting around a horizontal-axis since remanence acquisition, we calculated the expected remanence direction at 20 and 25 Ma from the apparent polar wander paths (APWP) of stable India (Acton, 1999; Besse and Courtillot, 2002) centered in the study area. The reference directions of the two APWP differ 3.7° for 20 Ma and 0.3° for 25 Ma and provide a high-quality reference point (Fig. 6b,f). Moreover the reference inclination has been calibrated taking into account 4.5 ± 0.5 cm/yr velocity of the northward drift of India–Asia since 20 Ma (Guillot et al., 2003) which yields 30° and 36° of inclination at 25 Ma and 20–15 Ma respectively.

6. Magnitude of vertical-axis rotation

As a first approximation for vertical-axis rotation in the area the mean of the pyrrhotite components for the 11 sites where compared with the expected direction at 25 Ma and 20 Ma from the two APWP (Table 1) (e.g. expected declination and inclination at 25 Ma are D/I = 001°/36°; Besse and Courtillot, 2002). The seven sites in the Qonggyai profile indicate a consistent trend of clockwise rotation ranging from 7° (site dq49) to 31° (site dq47) at 25 Ma (Fig. 8a). On the other hand different inclination values of the site mean directions are reflecting tilting around horizontal axes (Fig. 8c,d). The different inclination values and quite constant declination values of the site mean remanence vectors and single specimens ChRM directions result in a distribution along a great circle which can be well fitted using cylindrical best fit (Bingham analysis; Bingham, 1974). Directions are distributed within a great circle with maxima around 019° (eigenvector 1) (Fig. 6d). The angle of block rotation can be obtained when comparing the eigenvector 1 with the expected direction from the APWP (Fig. 6d). A clockwise block rotation of 18° is obtained for an expected remanence age of 25 Ma in the Qonggyai area. If the observed remanence directions are compared with an expected remanence acquisition age at 20 Ma a clockwise rotation of 17° and 14° will be obtained using APWPs Acton (1999) and Besse and Courtillot (2002), respectively (Figs. 6d and 1b). If the secondary remanence acquisition age occurred at ~15 Ma related to the contact metamorphism around the Yala Xiangbo dome, a clockwise rotation of 18°–15° is obtained.

In Nagarze area we obtained block rotation data at 3 points, site nn50, site nn60 and site dn1–dn2 (dn1 and dn2 sites were unified because their closer position). The mean site remanence directions indicate a lack of vertical-axis block rotations with respect to stable

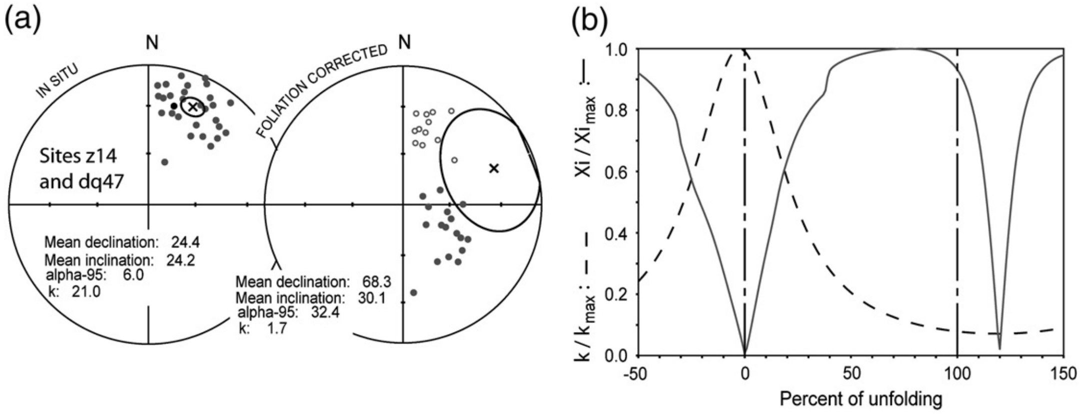

(c)

McFadden		In situ						After Tectonic correction					
n	CV Xi 95% lim.	D	I	alpha-95	k	Xi	MA	D	I	alpha-95	k	Xi	MA
29	6.155	24.4	24.2	6	21	0.2	after	68.3	30.1	32.4	1.7	26	after at 99% level

Max K						Min Xi					
D	I	alpha-95	k	Xi	MA unfolding	D	I	alpha-95	k	Xi	MA unfolding
24.4	23.9	6	21.2	1.846	-2%	24.4	24.2	6	21	0.2	0%

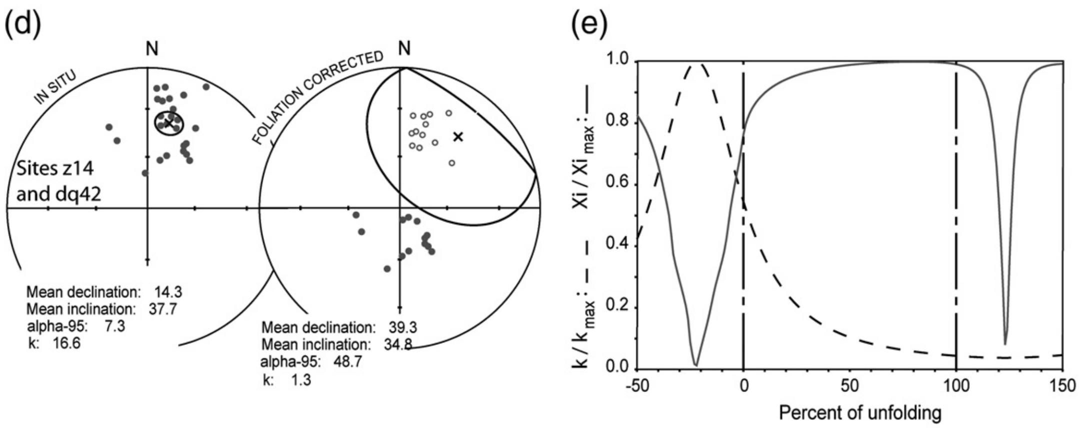

(f)

McFadden		In situ						After Tectonic correction					
n	CV Xi 95% lim.	D	I	alpha-95	k	Xi	MA	D	I	alpha-95	k	Xi	MA
25	5.82	14.3	37.3	7.3	16.6	18.4	before	39.3	34.8	48.7	1.3	23.9	after

Max K						Min Xi					
D	I	alpha-95	k	Xi	MA unfolding	D	I	alpha-95	k	Xi	MA unfolding
15.2	38.3	5.3	30.4	0.3	-22%	15.2	38.3	5.3	30.4	0.3	-22%

Fig. 7. Remanence directions and McFadden (1990) fold tests for the pyrrhotite component. Equal area projections of single specimen direction are shown before and after tectonic (foliation) correction. a) and b) for the D1 deformation domain (sites z14 and dq47). d) and e) for the D1 + D2 deformation domain (sites z14 and dq42). c) and f) show statistical parameters of McFadden algorithm.

India for a remanence acquisition age of 25–20 Ma (Figs. 1b and 8b). The same result is obtained when the 28 ChRM directions from individual specimens are fitted with Bingham statistics (1974). Declination of the eigenvector 1 of the cylindrical best fit is 001° which is equal to the expected direction (Fig. 6d).

7. Structures of last deformation phase and neotectonic markers

The area is structurally dominated by two sets of structures that control the surface processes. The analysis at 11 sites of tectonic markers witnessing the last deformation stage (D4) indicates the existence of E–W strike-slip faults while the sub N-trending structures are extensional faults (Fig. 9a). These structures cross-cut GCT, STDS and Yala Xiangbo dome and therefore must be post Late-Miocene to present. These structures are most probably coeval as has been previously described in the Bangong–Nujiang suture zone (e.g. Armijo et al., 1989; Taylor et al., 2003). Paleostress analyses were carried out at 6 sites where the inversion of fault striae, tension gashes and elongated quartz fibers was measured. Data density and quality are above average. TectonicsFP software was utilized for data processing (Ortner et al., 2002). The analyses show a regional N020° compression (P-axis) in agreement with present-day kinematics (e.g. Wang et al., 2001). The grain of the relief is marked by large ca. E–W trending faults, mainly the reactivation of older structures, such as the Yarlung Tsangpo suture, numerous sub N-trending faults of smaller extent and the 200 km long Cona Graben system (Fig. 9a; Armijo et al., 1989; Pan et al., 2004). These rifts are en-echelon and have a slight signature on the topography. Nonetheless, their traces can be determined with accuracy on a slope map and an incision map (Fig. 9a,b).

The ongoing deformation is attested by the strong river disequilibrium reflected e.g. in the Yarlung Tsangpo river longitudinal profile characteristic of river piracy (Fig. 9c). The knick-point K is located on the West Cona Graben shoulder (Fig. 9a). The shape of the strongly disequilibrated profile suggests that the E–W extension and the induced subsidence derived in a topographic gradient and a deepening of the base level of the river Yarlung Tsangpo. In turn, it triggered an

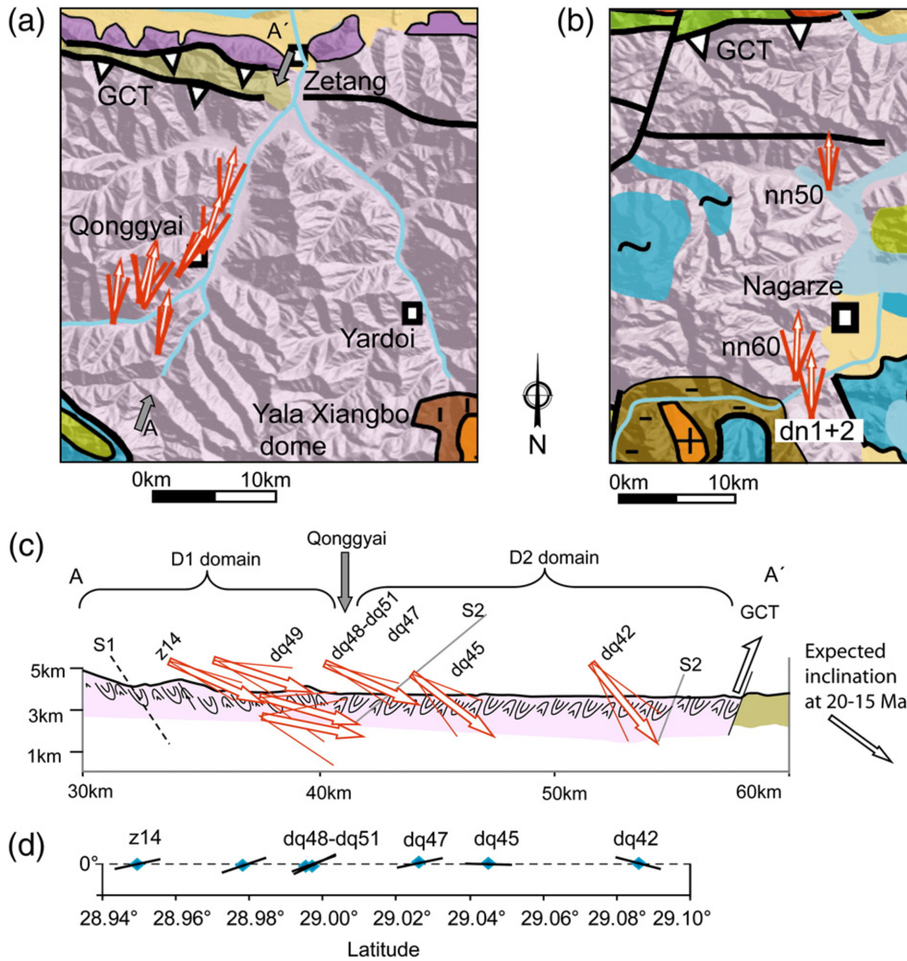

Fig. 8. Vertical axis block rotations and tilt around horizontal-axis. a) geological map overlapped with digital topography; arrows indicate angle of rotation versus stable India at 25 Ma in Qonggyai valley; cones show the confidence angle α_{95}/cos I. b) geological map overlapped with digital topography; arrows indicate angle of rotation versus stable India at 25 Ma in Nagarze area, cones represent confidence angles α_{95}/cos I. c) cross section along Qonggyai valley with observed inclinations from in situ mean directions of pyrrhotite components; black arrow show expected inclination (averaged from APWPs of Acton, 1999 and Besse and Courtillot, 2002). d) tilt around horizontal-axis values in the Qonggyai profile.

increased westward incision of the Yarlung Tsangpo and allowed the capture of a river previously flowing westward. This recent connection is attested by the angles between tributaries and the main river (Yarlung Tsangpo). Equilibrated rivers display a dendritic pattern where tributaries link to the main rivers at acute angles in the flow direction. In the west of the Cona Graben, the tributaries to the river Yarlung Tsangpo display acute angles towards west, probably witnessing a previous flow westwards. In the east of the Cona Graben the tributaries connect to the river Yarlung Tsangpo at expected east oriented acute angles.

The drainage system is largely controlled by the D4 structures. In a 50 km, E–W band centered by the Yarlung Tsangpo river, the rivers have an orthogonal pattern. Outside this band, the drainage network is dominantly sub-dendritic. The drainage system of Yarlung Tsangpo area is characterized by N–S elongated and pear-shaped watersheds and is bounded to the South by a NNW–SSE zone of N120 elongated watersheds parallel to the Lhunze fault (Fig. 9d,e). The southern segment of the Cona Graben system is characterized by N–S rectangular elongated watersheds (Fig. 9e). The basin asymmetries of the area indicate that the Yarlung Tsangpo area is dominated by E–W river offsets while the Cona Graben zones are mostly displaying N–S river offsets. The drainage system is indubitably under strong and active tectonic forcing. The basins forming the Cona Graben area are dextrally offset over E–W oriented faults. The vertical dissection and incision maps suggest an increasing trend of clockwise rotation of the Cona Graben segments to the north (Fig. 9a,b).

8. Discussion

8.1. Implications for eastward extrusion in SE Tibet

Taking into account that the remanence was acquired between 23 and 14 Ma the rotation angle can be interpreted in terms of vertical-axis block rotation related to slip along the ramp of the Great Counter Thrust (18–10 Ma; Harrison et al., 2000) or associated to post Late Miocene movements along strike-slip faults linked to E–W extension in the Himalaya and eastward extrusion of the Tibetan plateau (Tapponnier et al., 2001; Mahéo et al., 2007).

Taking into account that the movement of the hangingwall along the frontal ramp of the GCT was most probably frontal, and north-directed as indicated by stretching lineation values (N–S trend and 70° plunge towards the south; Montomoli et al., 2008; Antolín et al., in press) in the thrust zone, perpendicular to the thrust plane, block rotation are not expected by this process (Fig. 2a; for details about thrust ramp geometries and paleomagnetic vectors see Pueyo et al., 2003). However, our results fit well with the combined Quaternary strain rates and GPS velocity field which show an eastward regional motion of the upper crust (Fig. 1a; Holt et al., 2000; Gan et al., 2007). Rotation rates obtained from the GPS velocity field relative to Eurasia reflect a similar pattern with increasing clockwise rotation from the Nagarze–Yamdrock Lake area towards Qonggyai valley and the eastern syntaxis (Holt et al., 2000; Gan et al., 2007). Furthermore the neotectonic data suggest that the middle segment of the Cona

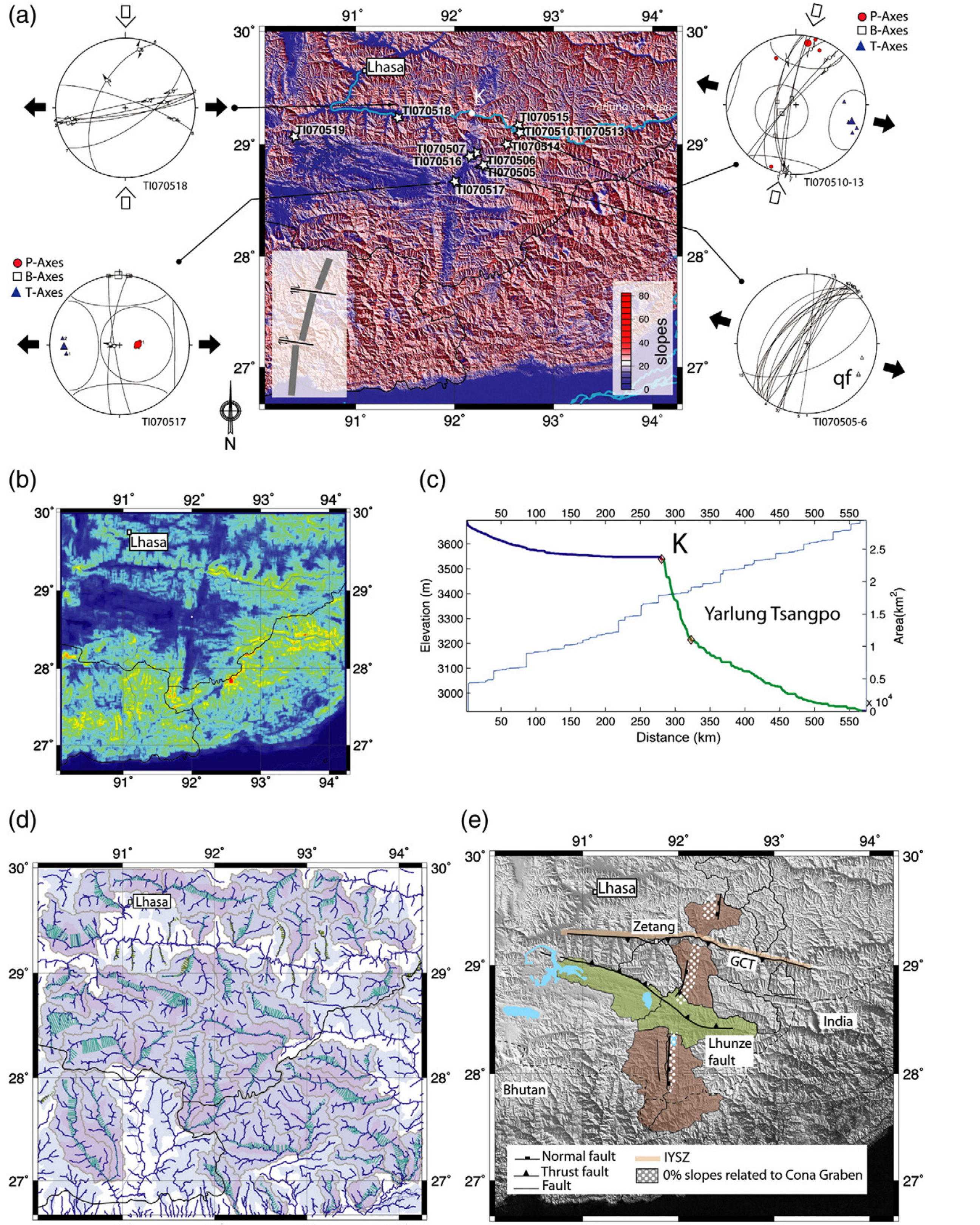

Fig. 9. D4 structures and geomorphological analysis. a) slope map draped on a shaded relief based on SRTM v.4 data. The numbers represent site locations where neotectonic markers were measured. Four representative structural analyses of D4 strain markers such as fault striae and tension gashes are displayed on the sides (black arrows: assumed maximum horizontal extensional stress direction, white arrows: assumed maximum horizontal compressive stress direction, qf: quartz fibers). In the right down part sketch of the Cona Graben en-echelon system (see text for further explanations). The light blue line represents the Yarlung Tsangpo river which profile is plotted in C. K is a major knick-point. b) incision map (local relief within 3 km). c) longitudinal profile of the Yarlung Tsangpo river in the study area and its contributing area. d) drainage system (dark blue lines represent the rivers of Strahler orders greater than 1, light blue shapes represent watersheds with Strahler order 2, gray contour shapes represent watersheds with Strahler order 3, the turquoise lines display the amount of offset between the main watershed rivers and the watershed symmetry axis. e) digital topography with the GCT, IYSZ, Lhunze fault and Cona Graben structures. Watersheds associated to the Lhunze fault in green color, watersheds associated to the Cona Graben in brown color.

Graben between the Indus Yarlung suture zone and the Lhunze fault have been 15°–20° clockwise rotated with respect to the southern segment (N–S oriented) (Figs. 9a,e and 10a,b).

We propose that the paleomagnetic ca. 20° vertical-axis clockwise rotation in the Qonggyai valley is the result of the strain partitioned between far-field stresses related to the SE extrusion, motion of the upper crust, of the southern part of the Tibetan plateau around the eastern syntaxis (Namche Barwa) and local strike-slip fault displacements (Fig. 10a,b). These occurred along the Indus Yarlung Tsangpo E–W right-lateral strike-slip faults (Armijo et al., 1989; Ratschbacher et al., 1994; Van der Woerd et al., 2009). This is supported by right-lateral transtensional markers observed in the field close to the suture zone (Fig. 9a).

Additional structural field work focused in the three different segments of the Cona Graben, the Lhunze fault and Yarlung Tsangpo suture are needed to better constrain their neotectonic importance. However the Lhunze fault appears like cutting the southern and middle segments of the Cona Graben and might have been reactivated as a strike-slip fault (Figs. 2a and 9e). The clockwise block rotation likely occurred during strike-slip displacements along the Indus Yarlung suture zone and the Lhunze fault (Fig. 10a,b).

The strike-slip faults are probably linked with E–W extension along the south Tibetan Grabens as pointed out by Taylor et al. (2003) (Fig. 10a,b). Onset of extension in the Tibetan plateau is still a matter of debate. On the central and southern Tibetan plateau 14–8 Ma ages have been proposed for the onset of graben formation (Harrison et al., 1995; Blisniuk et al., 2001). However west of the study area, within the Tethyan Himalaya, early Pliocene ages have been also described in the Kung Co half-Graben, close to Tingri (Mahéo et al., 2007) and associated to the onset of E–W extension. Reactivation of pre-existing weak structural zones as the IYSZ and the Lhunze fault might have played a significant role in the accommodation of E–W (or orogen-parallel) extension and eastward motion of the Tibetan plateau (e.g. Jessup et al., 2008; this study).

8.2. Implications for North Himalayan doming

Relative to the expected inclination at 20–15 Ma the observed inclinations in Qonggyai valley reflect a N–S pattern of tilt around the horizontal axis indicating a 15° tilting in site dq42, no tilting in site dq45 and a back-tilting south of it (Fig. 8c, d; Table 1). In Yamdrock Lake and Nagarze area an increasing degree of back-tilting can be observed from N to S approaching the Neogene leucogranite intrusion south of Nagarze. Taking into account that the sites in Qonggyai valley are 40 km WNW of the Yala Xiangbo dome and following the E–W lineament of the others North Himalayan domes, the tilt pattern can be interpreted as concealed doming. This is supported by the vitrinite reflectance values along the Qonggyai valley which indicate a maximum temperature and peak in the degree of metamorphism close to Qonggyai town which can be related to the roof of a deep-seated and not completely developed dome. This zone may have risen in Middle and Late Miocene times (Grujic et al., 2002), tilting and back-tilting the paleomagnetic vectors in the Qonggyai valley and close to Nagarze town around a ca. E–W horizontal axis (eigenvector 3 of the cylindrical best fit; Fig. 6d,f) coincident with the lineament of the outcropping domes. Fig. 10c,d sketch the supposed scenario for the observed inclination values.

9. Conclusions

The paleomagnetic data presented here allow us to separate a stable post-folding magnetization component in the Cretaceous diorite dykes emplaced in the Triassic turbiditic sediments, demagnetized in the pyrrhotite unblocking Curie temperature. Pyrrhotite

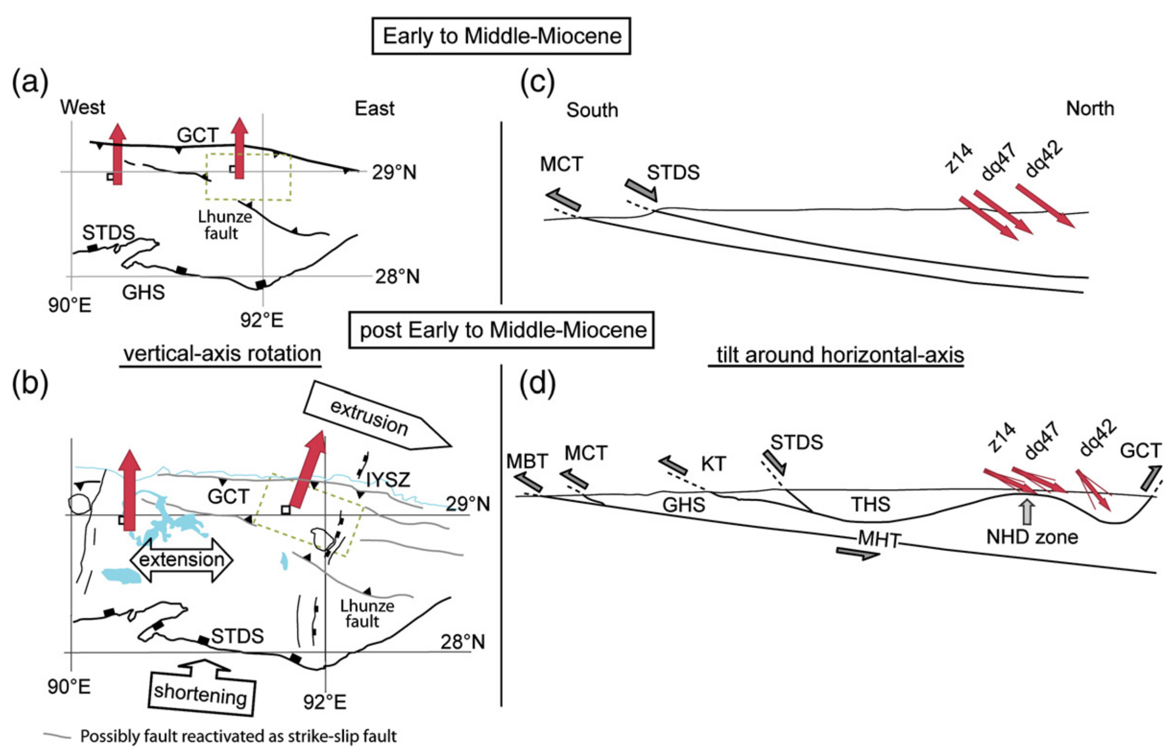

Fig. 10. Miocene kinematic model for the eastern Tethyan Himalaya. a) expected orientation of the paleomagnetic reference direction in the study area in Early and Middle–Miocene times within the structural frame (tectonic maps are simplified from Figs. 2 and 8). b) clockwise rotation of the pyrrhotite remanence directions in Qonggyai valley related to the strain partitioning and eastward extrusion of the Tibetan plateau. c) geodynamic scenario in Early and Middle–Miocene times with the expected inclination of the paleomagnetic vectors (schematic, interpretative, evolutionary cross-sections along A–A′ in Fig. 1b, slightly modified from Grujic et al., 2002). d) rise of the North Himalayan dome (NHD) zone in Middle and Late Miocene times could have induced tilting and back-tilting of the remanence vectors.

occurrence is supported by a Hopkinson peak and decay at 325 °C in high-temperature susceptibility curves, SIRM saturation field values >300mT, and a sharp decrease of remanent magnetization at ~325 °C during thermal demagnetization of the SIRM. A small contribution of magnetite is additionally present. The secondary character of the ChRM can be asserted by two facts: (i) Negative fold test for foliation attitudes of the D1 deformation phase domain and the D1 + D2 domain in the Qonggyai valley. (ii) Thermochronological data in the Triassic flysch indicating that a peak metamorphism above the Curie temperature of pyrrhotite was reached for the last time between 22 Ma and 14 Ma at the end of D2 tectonic phase (Aikman et al., 2004; Dunkl et al., 2008). Therefore the magnetization is of thermoremanent or thermo-chemical origin and can be evaluated as a record of the Early Miocene field.

Remanence vectors from Nagarze–Yamdrock Lake area and Qonggyai valley indicate a transition from no rotation in the west to ~20° clockwise rotation in the east against stable India since Early to Middle-Miocene. This rotation can be explained by the strong strain partitioning between far-field eastward extrusion and near-field strike-slip faulting and E–W extension reflected in the en-echelon Cona Graben system, the drainage system and the watersheds shape and distribution. At regional scale our results represent a field support for the clockwise rotation of the southeastern corner of the Tibetan plateau around the eastern syntaxis during the eastward extrusion, or motion of the upper crust, of the Tibetan plateau (Armijo et al., 1989; Royden et al., 1997; Tapponnier et al., 2001). However, more paleomagnetic and structural studies east of the Cona Graben should be done to verify this interpretation.

Tilting and back-tilting of the paleomagnetic remanence vectors around a horizontal-axis may reflect the rising of the North Himalayan dome zone in Middle Miocene times.

Acknowledgements

The authors are grateful for the aid during fieldwork to Tawa. We thank G. Ojha, P. Branscheid and L. Bello for assistance during the paleomagnetic measurements, and T. Frederichs for providing MPMS analysis. For standard paleomagnetic processing the Palmag software v.3.2 of Maier and Bachtadse and Stereonet for Windows v.1.2 of Allmendinger (2002–2003) were used. This research was supported by the German Science Foundation (DFG) in the frame of the Priority Programme 1372 “Tibetan Plateau: Formation, Climate, Ecosystems (TiP)” and by grants from the Chinese NSF (40625008 to Ding), CAS (KZCX2-YW-Q09-03 to Ding), and National Basic Research Program of China (2009CB421000 to Ding). We acknowledge the revision from two anonymous reviewers and the editor F. Storti who helped improve the first version of the manuscript.

References

Acton, G.D., 1999. Apparent polar wander of India since the Cretaceous with implications for regional tectonics and true polar wander. In: Radhakrishna, T., Piper, J.D.A. (Eds.), The Indian subcontinent and Gondwana; a paleomagnetic and rock magnetic perspective: Memoir-Geological Society of India, 44, pp. 129–175.

Aikman, A., Harrison, T.M., Lin, D., 2004. Preliminary results from the Yala-Xiangbo Leucogranite dome, SE Tibet. 19th Himalaya–Karakoram–Tibet workshop extended abstracts. Himalayan J. Sci. 2, 91.

Aikman, A., Harrison, T.M., Ding, L., 2008. Evidence for Early (>44 Ma) Himalayan Crustal Thickening, Tethyan Himalaya, southeastern Tibet. Earth Planet. Sci. Lett. 274, 14–23.

Antolín, B., Appel, E., Montomoli, C., Dunkl, I., Ding, L., Gloaguen R., El Bay, R. in press. Kinematic evolution of the eastern Tethyan Himalaya: Constraints from magnetic fabric and structural properties of the Triassic flysch in SE Tibet. In: J. Poblet and R. Lisle, Editors, Kinematic Evolution and Structural Styles of Fold-and-Thrust Belts, Geol. Soc. London Spec. Publ.

Ali, J.R., Aitchison, J.C., 2005. Greater India. Earth Sci. Rev. 72, 169–188.

Appel, E., Patzelt, A., Chouker, C., 1995. Secondary paleoremanence of Tethyan sediments from the Zanskar Range (NW Himalaya). Geophys. J. Int. 122, 227–242.

Armijo, R., Tapponnier, P., Mercier, J.L., Tonglin, H., 1986. Quaternary extension in southern Tibet: field observations and tectonic implications. J. Geophys. Res. 91 (nB14), 13803–13872.

Armijo, R., Tapponnier, P., Tonglin, H., 1989. Late Cenozoic right-lateral strike-slip faulting in Southern Tibet. J. Geophys. Res. 94, 2787–2838.

Besse, J., Courtillot, V., 2002. Apparent and true polar wander and the geometry of the geomagnetic field over the last 200 Myr. J. Geophys. Res. 107 (B11), 2300. doi:10.1029/2000jb000050.

Bingham, C., 1974. An antipodally symmetric distribution on the sphere. Ann. Stat. 2, 1201–1225.

Blisniuk, P.M., Hacker, B.R., Glodny, J., Ratschbacher, L., Bi, S., Wu, Z., McWilliams, M.O., Calvert, A., 2001. Extension in central Tibet since at least 13.5 Myr. Nature 412, 628–632.

Burbank, D., Meigs, A., Brozovi, N., 1996. Interactions of growing folds and coeval depositional Systems. Basin Res. 8, 199–223.

Burchfiel, B., Zhiliang, C., Hodges, K.V., Yuping, L., Royden, L.H., Changrong, D., Jiene, X., 1992. The South Tibetan detachment system, Himalaya orogen: extension contemporaneous with and parallel to shortening in a collisional mountain belt. Geol. Soc. Am. Spec. Pap. 269, 1–41.

Burg, J.P., Chen, G.M., 1984. Tectonics and structural zonation of southern Tibet, China. Nature 311, 219–223.

Carosi, R., Lombardo, B., Molli, G., Musumeci, G., Pertusati, P., 1998. The South Tibetan Detachment system in the Rongbuck valley, Everest region. Deformation features and geological implications. J. Asian Earth Sci. 16, 299–311.

Carosi, R., Montomoli, C., Visonà, D., 2002. Is there any detachment in the Lower Dolpo (western Nepal)? C.R. Geosci. 334, 933–940.

Cox, R.T., Van Arsdale, R.B., Harris, J.B., 2001. Identification of possible Quaternary deformation in the northeastern Mississippi Embayment using quantitative geomorphic analysis of drainage-basin asymmetry. Geol. Soc. Am. Bull. 113, 615–624.

Crouzet, C., Stang, H., Appel, E., Schill, E., Gautam, P., 2001. Detailed analysis of successive pTRMs carried by pyrrhotite in Himalayan metacarbonates: an example from Hidden Valley Central Nepal. Geophys. J. Int. 146, 607–618.

Crouzet, C., Gautam, P., Schill, E., Appel, E., 2003. Multicomponent magnetization in Western Dolpo (Tethyan Himalaya, Nepal): implications for tectonic motions. Tectonophysics 377, 179–196.

Ding, L., Kapp, P., Wan, X., 2005. Paleocene–Eocene record of ophiolite obduction and initial India–Asia collision, south central Tibet. Tectonics 24, TC3001. doi:10.1029/2004TC001729.

Dunkl, I., Lin, D., Montomoli, C., Wemmer, K., Rantisch, G., Antolín, B., El Bay, R., Appel, E., 2008. Diagenetic and metamorphic overprint and deformation history of Permo-Triassic Tethyan sediments, SE Tibet. 23th Himalaya–Karakoram–Tibet workshop extended abstracts. Himalayan J. Sci. 5, 49.

Dunkl, I., Antolín, B., Wemmer, K., Rantitsch, G., Kienast, M., Montomoli, C., Ding, L., Carosi, R., Appel, E., El Bay, R., Xu, Q. and von Eynatten, H., in press. Metamorphic evolution of the Tethyan Himalayan flysch in SE Tibet. In: R. Gloaguen and L. Ratschbacher, Editors, Growth and Collapse of the Tibetan Plateau, Geol. Soc. London Spec. Publ.

Dupuis, C., Hébert, R., Dubois-Coté, V., Guilmette, C., Wang, C.S., Li, Z.J., 2006. Geochemistry of sedimentary rocks from mélange and flysch units south of the Yarlung Zangbo suture zone, southern Tibet. J. Asian Earth Sci. 26, 489–508.

Eldredge, S., Bachtadse, V., Van der Voo, R., 1985. Paleomagnetism and the orocline hypothesis. Tectonophysics 119, 153–179.

Fisher, R.A., 1953. Dispersion on a sphere. Proc. R. Soc. London. 217, 295–305.

Gaetani, M., Garzanti, E., 1991. Multicyclic history of the northern Indian continental margin (northwestern Himalaya). AAPG Bull. 75, 1427–1446.

Gan, W., Zhang, P., Shen, Z.-K., Niu, Z., Wang, M., Wan, Y., Zhou, D., Cheng, J., 2007. Present-day crustal motion within the Tibetan Plateau inferred from GPS measurements. J. Geophys. Res. 112, B08416. doi:10.1029/2005JB004120.

Gansser, A., 1964. Geology of the Himalaya. Wiley-Interscience, New York. 289 pp.

Garzione, C.N., DeCelles, P.G., Hodkinson, D.G., Ojha, T.P., Upreti, B.N., 2003. East–west extension and Miocene environmental change in the southern Tibetan plateau: Thakkhola graben, central Nepal. Geol. Soc. Am. Bull. 115, 3–20.

Gloaguen, R., Marpu, P.R., Niemeyer, I., 2007. Automatic extraction of faults and fractal analysis from remote sensing data. Nonlinear Processes Geophys. 14 (2), 131–138.

Gloaguen, R., Käßner, A., Wobbe, F., Shahzad, F., Mahmood, A., 2008. Remote sensing analysis of crustal deformation using river networks. Geoscience and Remote Sensing Symposium. IGARSS 2008: IEEE International, 4, pp. 1–4.

Godin, L., 2003. Structural evolution of the Tethyan sedimentary sequence in the Annapurna area, central Nepal Himalaya. J. Asian Earth Sci. 22, 307–328.

Godin, L., Grujic, D., Law, R.D., Searle, M.P., 2006. Channel flow, extrusion and exhumation in continental collision zones: an introduction. In: Law, R.D., Searle, M.P., Godin, L. (Eds.), Channel Flow, Ductile Extrusion and Exhumation in Continental Collision Zones: Geol. Soc. London Spec. Publ., 268, pp. 1–23.

Grujic, D., Hollister, L.S., Parrish, R.R., 2002. Himalayan metamorphic sequence as an orogenic channel: insight from Bhutan. Earth Planet. Sci. Lett. 198, 177–191.

Guillot, S., Garzanti, G., Baratoux, D., Marquer, D., Maheo, G., de Sigoyer, J., 2003. Reconstructing the total shortening history of the NW Himalaya. Geochem. Geophys. Geosyst. 4. doi:10.1029/2002GC000484.

Harrison, T.M., Copeland, P., Kidd, W.S.F., Lovera, O.M., 1995. Activation of the Nyainqentanghla shear zone: Implications for uplift of the southern Tibetan Plateau. Tectonics 14, 658–676.

Harrison, T.M., Yin, A., Grove, M., Lovera, O.M., 2000. The Zedong Window: a record of superposed Tertiary convergence in southeastern Tibet. J. Geophys. Res. 105, 19211–19320.

Hodges, K.V., 2000. Tectonics of the Himalaya and southern Tibet from two perspectives. Geol. Soc. Am. Bull. 112, 324–350.

Holt, W.E., Chamot-Rooke, N., Le Pichon, X., Haines, A.J., Shen-Tu, B., Ren, J., 2000. Velocity field in Asia inferred from Quaternary fault slip rates and Global Positioning System observations. J. Geophys. Res. 105, 19185–19209.
Jackson, J., Norris, R., Youngson, J., 1996. The structural evolution of fault and fold systems in central Otago, New Zealand: evidence revealed by drainage patterns. J. Struct. Geol. 18, 217–234.
Jackson, J., Ritz, J.F., Siame, L., Raisbeck, G., Yiou, F., Norris, R.J., Youngson, J.H., Bennett, E., 2002. Fault growth and landscape development rates in Otago, New Zealand, using in situ cosmogenic 10Be. Earth Planet. Sci. Lett. 195, 185–193.
Jessup, M.J., Newell, D.L., Cottle, J.M., Berger, A.L., Spotila, J.A., 2008. Orogen-parallel extension and exhumation enhanced by focused denudation in the Arun River gorge, Ama Drime Massif, Tibet–Nepal. Geology 36, 587–590.
Käßner, A., Gloaguen, R., Stanek, K.-P., 2008. Remote sensing analysis of recent tectonics in the Eger Rift (Czech Republic). International Geoscience and Remote Sensing Symposium (IGARSS), pp. 1636–1639.
Kellett, D.A., Godin, L., 2009. Pre-Miocene deformation of the Himalayan superstructure, Hidden valley, central Nepal. J. Geol. Soc. London 166, 261–275.
Kellett, D.A., Grujic, D., Erdmann, S., 2009. Miocene structural reorganization of the South Tibetan detachment, eastern Himalaya: implications for continental collision. Lithosphere 1 (5), 259–281.
Kirschvink, J.L., 1980. The least-squares line and plane and the analysis of palaeomagnetic data. Geophys. J. R. Astron. Soc. 62, 699–718.
Klootwijk, C.T., Conaghan, P., Powell, C., 1985. The Himalayan Arc: large-scale continental subduction, oroclinal bending and back-arc spreading. Earth Planet. Sci. Lett. 75, 167–183.
Leech, M.L., 2008. Does the Karakoram fault interrupt mid-crustal channel flow in the western Himalaya? Earth Planet. Sci. Lett. 276, 314–322.
Lee, J., Hacker, B.R., Dinklage, W.S., Wang, Y., Gans, P., Calvert, A., Wan, J.L., Chen, W.J., Blythe, A.E., McClelland, W., 2000. Evolution of the Kangmar Dome, southern Tibet: structural, petrologic, and thermochronologic constraints. Tectonics 19, 872–895.
Li, D., Yin, A., 2008. Orogen-parallel, active left-slip faults in the Eastern Himalaya: implications for the growth mechanism of the Himalayan Arc. Earth Planet. Sci. Lett. 274, 258–267.
Liebke, U., Appel, E., Neumann, U., Antolin, B., Ding, L, Xu, Q., in press. Position of the Lhasa terrane prior to India–Asia collision derived from palaeomagnetic inclinations of 53 Ma old dykes of the Linzhou Basin: constraints on the age of collision and post-collisional shortening within the Tibetan Plateau. Geophys. J. Int. doi:10.1111/j.1365-246X.2010.04698.x.
Liu, G., Einsele, G., 1994. Sedimentary history of the Tethyan basin in the Tibetan Himalayas. Geol. Rundsch. 83, 32–61.
Maffione, M., Speranza, F., Faccenna, C., Rosello, E., 2009. Paleomagnetic evidence for a pre-early Eocene (50 Ma) bending of the Patagonian orocline (Tierra del Fuego, Argentina): Paleogeographic and tectonic implications. Earth Planet. Sci. Lett. doi:10.1016/j.epsl.2009.11.015.
Mahéo, G., Leloup, P.H., Valli, F., Lacassin, R., Arnaud, N., Paquette, J.-L., Fernandez, A., Haibing, L., Farley, K.A., Tapponnier, P., 2007. Post 4 Ma initiation of normal faulting in southern Tibet. Constraints from the Kung Co half graben. Earth Planet. Sci. Lett. 256, 233–243.
McFadden, P.L., 1990. A new fold test for paleomagnetic studies. Geophys. J. Int. 103, 163–169.
Montomoli, C., Appel, E., Antolín, B., Dunkl, I., El Bay, R., Lin, D., Gloaguen, R., 2008. Polyphase deformation history of the "Tibetan Sedimentary Sequence" in the Himalaya chain (South-East Tibet). 23th Himalaya–Karakoram–Tibet workshop extended abstracts. Himalayan J. Sci. 5, 91.
Nagata, T., 1961. Rock Magnetism, 2nd edition. Maruzen, Tokyo, p. 350.
Oliva-Urcia, B., Pueyo, E.L., 2007. Rotational basement kinematics deduced from remagnetized cover rocks (Internal Sierras, southwestern Pyrenees). Tectonics 26, TC4014.
Ortner, H., Reiter, F., Acs, P., 2002. Easy handling of tectonic data: the programs TectonicVB for Mac and TectonicsFP for Windows. Comput. Geosci. (28/10), 1193–1200. doi:10.1016/S0098-3004(02)00038-9.
Pan, G., Ding, J., Yao, D., Wang, L., 2004. Geological map of Qinghai–Xizang (Tibet) Plateau and Adjacent Areas (1:1,500,000). Chengdu Institute of Geology and Mineral Resources, China Geological Survey. Chengdu Cartographic Publishing House.
Pêcher, A., Bouchez, J.L., Le Fort, P., 1991. Miocene dextral shearing between Himalaya and Tibet. Geology 19, 683–685.
Pueyo, E.L., Pocoví, A., Parés, J.M., Millán, H., Larrasoaña, J.C., 2003. Thrust ramp geometry and spurious rotations of paleomagnetic vectors. Stud. Geophys. Geod. 47, 331–357.
Ratschbacher, L., Frisch, W., Liu, G., Chen, C., 1994. Distributed deformation in southern and western Tibet during and after the India–Asia collision. J. Geophys. Res. Solid Earth 99, 19917–19945.
Rochette, P., Fillion, G., Mattéi, J.L., Dekkers, M.J., 1990. Magnetic transition at 30–34 Kelvin in pyrrhotite: insight into widespread occurrence of this mineral in rocks. Earth Planet. Sci. Lett. 98, 319–328.
Royden, L.H., Burchfiel, B.H., King, R.W., Wang, E., Chen, Z., Shen, F., Liu, Y., 1997. Surface deformation and lower crustal flow in Eastern Tibet. Science 276, 788–790.
Schill, E., Appel, E., Zeh, O., Singh, V.K., Gautam, P., 2001. Coupling of late-orogenic tectonics and secondary pyrrhotite remanences: towards a separation of different rotation processes and quantification of rotational underthrusting in the western Himalayas (N-India). Tectonophysics 337, 1–21.
Schill, E., Holt, W.E., 2004. 20 Ma of lateral mass transfer around the western Himalayan syntaxis. Extended abstracts: 19th Himalaya–Karakoram–Tibet Workshop, Niseko, Japan. 19th Himalaya–Karakoram–Tibet workshop extended abstracts. Himalayan J. Sci. 2 (4), 244–245.
Schill, E., Appel, E., Crouzet, C., Gautam, P., Wehland, F., Staiger, M., 2004. Oroclinal bending versus regional significant clockwise rotations in the Himalayan arc-Constrains from secondary pyrrhotite remanences. In: Sussman, A.J., Weil, A.B. (Eds.), Orogenic Curvature: Integrating Paleomagnetic and Structural Analyses: Spec. Pap. Geol. Soc. Am., 383, pp. 73–85.
Searle, M.P., 1996. Cooling history, erosion, exhumation and kinematics of the Himalaya–Karakoram–Tibet orogenic belt. In: Yin, A., Harrison, T.M. (Eds.), Tectonics of Asia. Rubey Symposium volume, Los Angeles, pp. 110–137.
Shahzad, F., Mahmood, S.A., Gloaguen, R., 2009. Drainage network and lineament analysis: an approach for Potwar Plateau (Northern Pakistan). J. Mt. Sci. 6 (1), 14–24.
Shahzad, F., Gloaguen, R., in press-a. Understanding tectonics from digital elevation model, part 1: Drainage network preparation and stream profile analysis. Computer and Geosciences.
Shahzad, F., Gloaguen, R., in press-b. Understanding tectonics from digital elevation model, part 2: Surface dynamics and basin analysis. Computer and Geosciences.
Tapponnier, P., Peltzer, G., Le Dain, A.Y., Armijo, R., Cobbold, P., 1982. Propagating extrusion tectonics in Asia: new insights from simple experiments with plasticine. Geology 10, 611–616.
Tapponnier, P., Zhiqin, X., Roger, F., Meyer, B., Arnaud, N., Wittlinger, G., Jingsui, Y., 2001. Oblique stepwise rise and growth of the Tibet Plateau. Science 294, 1671–1677.
Taylor, M., Yin, A., Ryerson, J.F., Kapp, P., Ding, L., 2003. Conjugate strike-slip faulting along the Bangong–Nujiang suture zone accommodates coeval east–west extension and north–south shortening in the interior of the Tibetan Plateau. Tectonics 22 (4), 1044. doi:10.1029/2002TC001361, 2003.
Van der Woerd, J., Leloup, Ph.-H., Liu-Zeng, J., Lacassin, R., Tapponnier, P., 2009. A comment on "Orogen-parallel, active left-slip faults in the eastern Himalaya: Implications for the growth mechanism of the Himalayan arc" by Li and Yin. Earth Planet. Sci. Lett. 278, 258–267 Earth Planet. Sci. Lett. 285, 217–222.
Wang, Q., Zhang, P.Z., Freymueller, J.T., Bilham, R., Kristine, K.M., Lai, X., You, X., Niu, Z., Wu, J., Li, Y., Liu, J., Yang, Z., Chen, Q., 2001. Present-day crustal deformation in China constrained by global positioning system measurements. Science 294, 574–577.
Weil, A.B., Sussman, A.J., 2004. Classifying curved orogens based on timing relationships between structural development and vertical-axis rotations. In: Sussman, A.J., Weil, A.B. (Eds.), Spec. Pap. Geol. Soc. Am., 383, pp. 1–15.
Willems, H., Zhou, Z., Zhang, B., Gräfe, K.U., 1996. Stratigraphy of the Upper Cretaceous and Lower Tertiary strata in the Tethyan Himalayas of Tibet (Tingri area, China). Geol. Rundsch. 85, 723–754.
Yin, A., Harrison, T.M., Ryerson, F.J., Wenji, C., Kidd, W., Copeland, P., 1994. Tertiary structural evolution of the Gangdese thrust system, southeastern Tibet. J. Geophys. Res. 99, 18.175–18.201.
Yin, A., Harrison, T.M., 2000. Geologic evolution of the Himalayan–Tibetan orogen. Annu. Rev. Earth Planet. Sci. 28, 211–280.
Zhang, P.Z., Shen, Z., Wang, M., Gan, W., Bürgmann, R., Molnar, P., Wang, Q., Niu, Z., Sun, J., Wu, J., Hanrong, S., Xinzhao, Y., 2004. Continuous deformation of the Tibetan Plateau from global positioning system data. Geology 32, 809–812.
Zhu, D., Mo, X., Pan, G., Zhao, Z., Dong, G., Shi, Y., Liao, Z., Wang, L., Zhou, C., 2008. Petrogenesis of the earliest Early Cretaceous mafic rocks from the Cona area of the eastern Tethyan Himalaya in south Tibet: interaction between the incubating Kerguelen plume and the eastern Greater India lithosphere? Lithos 100, 147–173.
Xu, X., Ding, L., Xu, Q., Cai, F., Zhang, Q., Zhang, L., Lai, Q., 2009. Tectonics implications of the Ultramafic Dykes in Southeastern Tibet. Chinese J. Geol. 44, 1012–1024 (in Chinese with English abstract).